Attitude determination with low-cost GPS/ INS

P. Henkel[*,**] and C. Günther[*,**,***]
[*] *Technische Universität München (TUM), Munich, Germany*
[**] *Advanced Navigation Solutions - ANAVS, Munich, Germany*
[***] *German Aerospace Center (DLR), Oberpfaffenhofen, Germany*

BIOGRAPHIES

Patrick Henkel received his Bachelor, Master and PhD degrees from the Technische Universität München, Munich, Germany. In 2010, he graduated with a PhD thesis on reliable carrier phase positioning, which received with "summa cum laude" the highest distinction. Patrick is now working towards his habilitation in the field of precise point positioning. He visited the Mathematical Geodesy and Positioning group at TU Delft in 2007, and the GPS Lab at Stanford University in 2008 and 2010. Patrick received the Pierre Contensou Gold Medal in 2007, the 1st prize in Bavaria at the European Satellite Navigation Competition in 2010, and the Vodafone Award for his dissertation in 2011. He is one of the founders and currently also the managing director of Advanced Navigation Solutions - ANAVS.

Christoph Günther studied theoretical physics at the Swiss Federal Institute of Technology in Zurich. He received his diploma in 1979 and completed his PhD in 1984. He worked on communication and information theory at Brown Boveri and Ascom Tech. From 1995, he led the development of mobile phones for GSM and later dual mode GSM/Satellite phones at Ascom. In 1999, he became head of the research department of Ericsson in Nuremberg. Since 2003, he is the director of the Institute of Communication and Navigation at the German Aerospace Center (DLR) and since December 2004, he additionally holds a Chair at the Technische Universität München (TUM). His research interests are in satellite navigation, communication and signal processing.

ABSTRACT

Low-cost GNSS receivers with patch antennas track the carrier phases of the GNSS signals with millimeter- to centimeter-level accuracy. However, code multipath of several tens of metres, frequent half cycle slips, and receiver clock offsets in the order of milliseconds make reliable kinematic integer ambiguity resolution still challenging.

Low-cost inertial sensors are robust against GNSS signal shadowing and benefit from a higher measurement rate but show large integration drifts due to biases in the gyroscope and acceleration measurements and, require an initialization with another sensor.

In this paper, we couple the information of both sensors for attitude determination and propose a search algorithm for cycle slip detection and correction. The search algorithm uses double difference carrier phase, acceleration and gyroscope measurements, and also considers a priori information on the baseline length. The cycle slip corrections are determined such that the optimum trade-off between minimizing the squared measurement residuals and minimizing the squared baseline length residuals is found. We tested the method during various car drives. Measurement results show that the method reliably corrects all cycle slips in environments with both high multipath and high receiver dynamics, and enables a heading determination with an accuracy of $0.5^\circ/$ baseline length [m].

INTRODUCTION

Attitude determination is widely performed with inertial sensors and geodetic GNSS receivers in maritime and aerospace applications. The carrier phase can be tracked with millimeter-level accuracy and, therefore, is very attractive for precise attitude determination. Double differences are formed to eliminate receiver and satellite clock offsets and biases as well as atmospheric errors. This leaves the double difference integer ambiguities and baseline coordinates as unknowns. Teunissen developed the Least Squares Ambiguity Decorrelation Adjustment (LAMBDA) method in [1] to solve the integer least-squares problem. For attitude determination, the success rate of ambiguity resolution can be further increased if the baseline length a priori information is included in the search process. In [2] and [3], Teunissen developed a constrained LAMBDA method to solve the constrained integer least-squares problem.

Low-cost GNSS receivers can also track the carrier pha-

se with millimeter- to centimeter-level accuracy. Consequently, they are very attractive for automotive applications (e.g. heading determination of cars, Fig. 1).

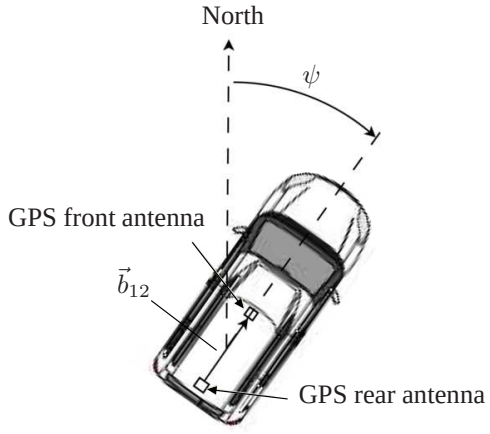

Fig. 1: Heading determination of a car with two GPS receivers mounted on the roof of the car.

However, there are three fundamental differences between attitude determination with geodetic and low-cost single-frequency GNSS receivers and antennas. Tab. 1 lists the challenges of low-cost GNSS receivers/ antennas (e.g. u-blox, Skytraq) and our approach to overcome them.

Tab. 1: Challenges of attitude determination with low-cost GPS receivers and antennas

- oscillators:
  receiver clock offsets in the order of milliseconds compared to nanoseconds for geodetic receivers, double difference ambiguity no longer integer valued
  our solution:
  correction of satellite movement within time of differential receiver clock offset [4]

- code multipath:
  10 m in good environments and
  50 m in challenging environments
  our solution:
  use of code measurements only for initial ambiguity fixing,
  careful selection of satellites and epochs based on residuals

- cycle slips:
  very frequent, half cycle slips, also affecting multiple satellites simultaneously, and difficult to distinguish from dynamics and phase multipath
  our solution:
  integer search using low-cost IMU and baseline length a priori information,
  elevation mask of 20°

We model the double difference carrier phase measurements as proposed by Henkel, Giorgi and Günther in [4] and by Henkel and Oku in [5] as

$$\begin{aligned}
&\big(\lambda\varphi_1^k(t+\delta\tau_1) - \lambda\varphi_1^l(t+\delta\tau_1)\big)\\
&-\big(\lambda\varphi_2^k(t+\delta\tau_2) - \lambda\varphi_2^l(t+\delta\tau_2)\big)\\
&= \quad \|\vec{x}_1(t+\delta\tau_1) - \vec{x}^{\,k}(t+\delta\tau_1-\Delta\tau_1^k)\|\\
&\quad - \|\vec{x}_1(t+\delta\tau_1) - \vec{x}^{\,l}(t+\delta\tau_1-\Delta\tau_1^l)\|\\
&\quad - \|\vec{x}_2(t+\delta\tau_2) - \vec{x}^{\,k}(t+\delta\tau_2-\Delta\tau_2^k)\|\\
&\quad + \|\vec{x}_2(t+\delta\tau_2) - \vec{x}^{\,l}(t+\delta\tau_2-\Delta\tau_2^l)\|\\
&\quad + \lambda N_{12}^{kl} + \lambda/2\Delta N_{12}^{kl}(t) + m_{12}^{kl}(t+\delta\tau_1, t+\delta\tau_2)\\
&\quad + \varepsilon_{12}^{kl}(t+\delta\tau_1, t+\delta\tau_2), \qquad (1)
\end{aligned}$$

with the carrier wavelength λ, the carrier phase measurement φ_r^k of receiver r and satellite k, the receiver clock offset $\delta\tau_r$, the receiver position $\vec{x}_r$, the satellite position $\vec{x}^{\,k}$, the double difference (DD) integer ambiguity N_{12}^{kl}, the half cycle slip ΔN_{12}^{kl}, the phase multipath m_{12}^{kl} and the phase noise ε_{12}^{kl}.

We apply the synchronization correction of [4] to Eq. (1) and consider a static vehicle such that DD cycle slips can be easily corrected using triple difference phase measurements. After synchronization and cycle slip correction, the double difference measurement model simplifies to

$$\lambda\varphi_{12}^{kl} = \vec{e}^{\,kl}\vec{b}_{12} + \lambda N_{12}^{kl} + \varepsilon_{12}^{kl}, \qquad (2)$$

with $\vec{e}^{\,kl}$ being the difference in unit vectors pointing from satellites k and l to the receivers and $\vec{b}_{12}$ being the baseline vector between both receivers. The baseline coordinates and DD integer ambiguities are then determined by a constrained integer least-squares estimation, i.e.

$$\begin{aligned}
&\min_{\vec{b}_{12}, N_{12}} \left\| \begin{pmatrix} \lambda\varphi_{12} \\ \rho_{12} \end{pmatrix} - H\vec{b}_{12} - AN_{12} \right\|^2_{\Sigma^{-1}_{\varphi_{12}}}\\
&\quad \text{s.t.} \quad \|\vec{b}_{12}\| \stackrel{!}{=} l, \qquad (3)
\end{aligned}$$

where $\lambda\varphi_{12}$ and ρ_{12} include the DD phase and code measurements (here: of 500 epochs (100 s)), N_{12} is the vector of double difference integer ambiguities, H and A describe the mapping of the baseline/ ambiguity parameters to the measurements, $\Sigma_{\varphi_{12}}$ is the covariance matrix of the double difference phase and code measurements, and l includes the baseline length a priori information.

The optimization of Eq. (3) requires a constrained tree search as described in details in [6] and [4]. Once the ambiguities are resolved, we perform a precise coasting of the baseline solution as described in [7]. Finally, we transform the baseline estimates from the ECEF e-frame to the local (ENU) navigation (n-) frame, i.e.

$$\begin{aligned}
\hat{\vec{b}}^{\,\mathrm{n}}_{12} &= l \cdot \begin{pmatrix} \cos(\theta)\sin(\psi) \\ \cos(\theta)\cos(\psi) \\ \sin(\theta) \end{pmatrix} = C_{\mathrm{e}}^{\mathrm{n}}\hat{\vec{b}}_{12}\\
&= R_1(\pi/2-\varphi)R_3(\pi/2+\lambda)\hat{\vec{b}}_{12}, \qquad (4)
\end{aligned}$$

where φ and λ are the latitude and longitude of the receiver, R_i describes the rotation around the i-th axis, and ψ and θ are the heading and pitch angles. These angles can be directly derived from Eq. (4) as

$$\begin{aligned} \psi &= \operatorname{atan}\left((\hat{\vec{b}}^{\mathrm{n}}_{12})_x / (\hat{\vec{b}}^{\mathrm{n}}_{12})_y\right) \\ \theta &= \operatorname{atan}\left((\hat{\vec{b}}^{\mathrm{n}}_{12})_z / \sqrt{((\hat{\vec{b}}^{\mathrm{n}}_{12})_x)^2 + ((\hat{\vec{b}}^{\mathrm{n}}_{12})_y)^2}\right). \end{aligned} \quad (5)$$

We have tested the initial integer ambiguity resolution and subsequent phase coasting at the garden of *Nymphenburg palace* in Munich, Germany. Fig. 2 shows the track of the vehicle in the garden with good satellite visibility and limited multipath.

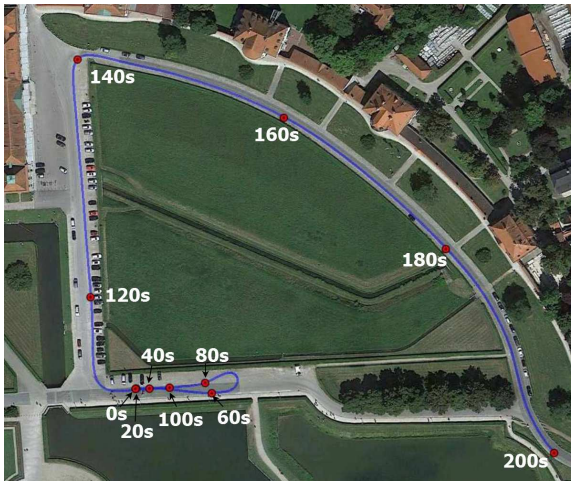

Fig. 2: Track of car drive at Nymphenburg palace with good satellite visibility and limited multipath. The track is subdivided into sections of 20 s.

Fig. 3 and 4 show the obtained heading and fixed phase residuals. One can observe that the noise level of the heading estimate is in the order of only $0.1°$. The phase residuals of all double differences are in the order of only a few centimeters throughout the measurement period, which indicates a correct integer ambiguity resolution.

KINEMATIC CYCLE SLIP DETECTION AND CORRECTION

Let us now consider a kinematic case in a more challenging environment. We assume that a synchronization correction has been applied to the double difference (DD) carrier phase measurements φ^{kl}_{12} and that their ambiguities $\check{N}^{kl}_{12}$ have been fixed. The synchronized and fixed DD carrier phases are then be modeled as

$$\lambda(\varphi^{kl}_{12} - \check{N}^{kl}_{12}) = \vec{e}^{\,kl}\vec{b}_{12} + \lambda/2\Delta N^{kl}_{12} + m^{kl}_{12} + \varepsilon^{kl}_{12}. \quad (6)$$

If the baseline is predicted from the last epoch to the current one using the IMU, then the cycle slip correction (CSC) is

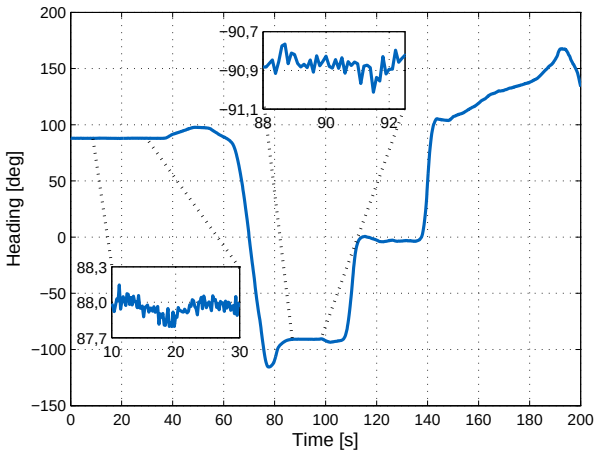

Fig. 3: Heading of track at Nymphenburg palace: The noise of the heading estimate is in the order of only $0.1°$.

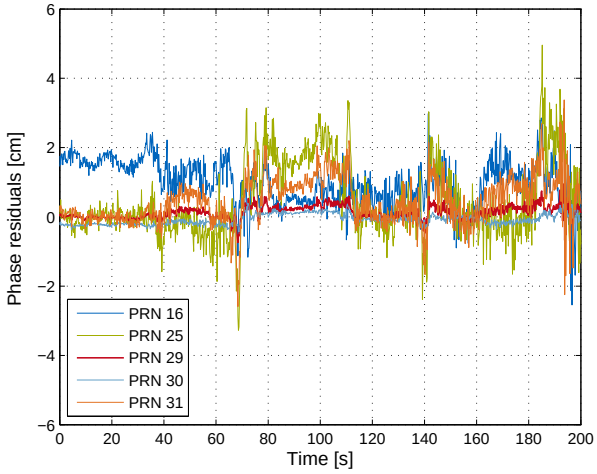

Fig. 4: Phase residuals of fixed baseline solution for track at Nymphenburg: The phase residuals of all satellites are far below one wavelength, which indicates a correct initial ambiguity resolution and a correct detection and correction of all cycle slips.

easily found by solving (6) for ΔN^{kl}_{12}, i.e.

$$\Delta\check{N}^{kl}_{12} = \left[\frac{1}{\lambda/2}\left(\lambda(\varphi^{kl}_{12} - \check{N}^{kl}_{12}) - \vec{e}^{\,kl}\hat{\vec{b}}^{\mathrm{IMU}}_{12}\right)\right]. \quad (7)$$

However, the CSC of (7) becomes critical if the initial alignment and/ or the calibration of the IMU was not sufficiently accurate. In this case, the alignment and calibration of the IMU has to be improved (e.g. in a tightly coupled solution) or an extended search using further information (e.g. on the baseline length) has to be performed. We consider the second case.

IMPROVED KINEMATIC CYCLE SLIP DETECTION AND CORRECTION

We would like to improve the CSC by a joint processing of the fixed DD phase measurements from all satellites. We additionally extend the measurement vector by including the baseline estimate of the IMU, i.e.

$$z = \begin{pmatrix} \lambda(\varphi_{12} - \check{N}_{12}) \\ \hat{\vec{b}}_{12}^{\mathrm{IMU}} \end{pmatrix}, \tag{8}$$

with φ_{12} and $\check{N}_{12}$ being the stacked DD carrier phases and ambiguities from all available satellites with a common reference satellite. As satellite availability is a critical issue in urban environments, we consider only a two-dimensional horizontal baseline vector. A baseline estimate is obtained from the a priori known baseline length l and the predicted heading ψ, i.e.

$$\hat{\vec{b}}_{12}^{\mathrm{IMU}} = l \cdot \begin{pmatrix} \sin(\psi) \\ \cos(\psi) \end{pmatrix}. \tag{9}$$

Initial alignment of IMU

We start with a rough alignment by transforming the measured acceleration a^{s} and angular rotation rate ω^{s} from the sensor-fixed (s-) frame to the body-fixed (b-) frame, i.e.

$$\begin{aligned} a^{\mathrm{b}}_{\mathrm{rough}} &= C^{\mathrm{b}}_{\mathrm{s}}\omega^{\mathrm{s}} = R_1(\phi^{\mathrm{b}}_{\mathrm{s}})R_2(\theta^{\mathrm{b}}_{\mathrm{s}})R_3(\psi^{\mathrm{b}}_{\mathrm{s}})a^{\mathrm{s}} \\ \omega^{\mathrm{b}}_{\mathrm{rough}} &= C^{\mathrm{b}}_{\mathrm{s}}\omega^{\mathrm{s}} = R_1(\phi^{\mathrm{b}}_{\mathrm{s}})R_2(\theta^{\mathrm{b}}_{\mathrm{s}})R_3(\psi^{\mathrm{b}}_{\mathrm{s}})\omega^{\mathrm{s}}, \end{aligned} \tag{10}$$

where the roll angle $\phi^{\mathrm{b}}_{\mathrm{s}}$, the pitch angle $\theta^{\mathrm{b}}_{\mathrm{s}}$ and the yaw angle $\psi^{\mathrm{b}}_{\mathrm{s}}$ are approximated from the mounting of the sensor on the body. Subsequently, we average $\omega^{\mathrm{b}}_{\mathrm{rough}}$ in static conditions to determine the biases b^{b}_{ω}, which are then subtracted from the measurements:

$$\omega^{\mathrm{b}} = \omega^{\mathrm{b}}_{\mathrm{rough}} - b^{\mathrm{b}}_{\omega}. \tag{11}$$

The acceleration measurements are also averaged over time in static conditions to reduce the noise. The obtained $\bar{a}^{\mathrm{b}}$ is expressed in terms of the Euler angles ϕ, θ, ψ and the gravitational acceleration g, i.e.

$$\begin{aligned} \bar{a}^{\mathrm{b}} &= C^{\mathrm{b}}_{\mathrm{n}}\bar{a}^{\mathrm{n}} \\ &\approx R_1(\phi)R_2(\theta)R_3(\psi)(0,0,g)^{\mathrm{T}} \\ &= \begin{pmatrix} -\sin(\theta) \\ \cos(\theta)\sin(\phi) \\ \cos(\theta)\cos(\phi) \end{pmatrix} \cdot g. \end{aligned} \tag{12}$$

The roll and pitch angles can then be derived from Eq. (12) without the need of knowing g as

$$\begin{aligned} \phi &= \mathrm{atan}\left(\bar{a}^{\mathrm{b}}_y / \bar{a}^{\mathrm{b}}_z\right) \\ \theta &= \mathrm{atan}\left(-\bar{a}^{\mathrm{b}}_x / \sqrt{(\bar{a}^{\mathrm{b}}_y)^2 + (\bar{a}^{\mathrm{b}}_z)^2}\right). \end{aligned} \tag{13}$$

We obtained the initial heading angle ψ from Eq. (5). Once the Euler angles and a rough estimate of the absolute position (longitude λ, latitude φ) is available from GPS, the coordinate frame transformation from the b-frame to the ECEF e-frame is determined as

$$C^{\mathrm{e}}_{\mathrm{b}} = C^{\mathrm{e}}_{\mathrm{n}} C^{\mathrm{n}}_{\mathrm{b}} \tag{14}$$

with

$$C^{\mathrm{e}}_{\mathrm{n}} = \begin{pmatrix} -\sin(\varphi)\cos(\lambda) & -\sin(\lambda) & -\cos(\varphi)\cos(\lambda) \\ -\sin(\varphi)\sin(\lambda) & \cos(\lambda) & -\cos(\varphi)\sin(\lambda) \\ \cos(\varphi) & 0 & -\sin(\varphi) \end{pmatrix} \tag{15}$$

and

$$C^{\mathrm{n}}_{\mathrm{b}} = (C^{\mathrm{b}}_{\mathrm{n}})^{-1} = (R_1(\phi)R_2(\theta)R_3(\psi))^{-1}. \tag{16}$$

The rotation matrix $C^{\mathrm{b}}_{\mathrm{e}} = (C^{\mathrm{e}}_{\mathrm{b}})^{-1}$ is then transformed to a Quaternion as described by Jekeli in [8], i.e.

$$q = \frac{1}{\|[q_a, q_b, q_c, q_d]\|} \cdot [q_a, q_b, q_c, q_d]^{\mathrm{T}} \tag{17}$$

with the four quaternion elements

$$\begin{aligned} q_a &= \frac{1}{2}\sqrt{1 + (C^{\mathrm{b}}_{\mathrm{e}})_{(1,1)} + (C^{\mathrm{b}}_{\mathrm{e}})_{(2,2)} + (C^{\mathrm{b}}_{\mathrm{e}})_{(3,3)}} \\ q_b &= \frac{1}{4q_a}((C^{\mathrm{b}}_{\mathrm{e}})_{(3,2)} - (C^{\mathrm{b}}_{\mathrm{e}})_{(2,3)}) \\ q_c &= \frac{1}{4q_a}((C^{\mathrm{b}}_{\mathrm{e}})_{(1,3)} - (C^{\mathrm{b}}_{\mathrm{e}})_{(3,1)}) \\ q_d &= \frac{1}{4q_a}((C^{\mathrm{b}}_{\mathrm{e}})_{(2,1)} - (C^{\mathrm{b}}_{\mathrm{e}})_{(1,2)}). \end{aligned} \tag{18}$$

Orientation integration

Jekeli derived the time-derivative of $C^{\mathrm{b}}_{\mathrm{e}}$ in [8] as

$$\dot{C}^{\mathrm{b}}_{\mathrm{e}} = C^{\mathrm{b}}_{\mathrm{e}}\Omega^{\mathrm{e}}_{\mathrm{be}}, \tag{19}$$

which represents a differential equation with unknown $C^{\mathrm{b}}_{\mathrm{e}}$. The skew-symmetric matrix $\Omega^{\mathrm{e}}_{\mathrm{be}}$ is given by

$$\Omega^{\mathrm{e}}_{\mathrm{be}} = \begin{pmatrix} 0 & -\omega_3 & \omega_2 \\ \omega_3 & 0 & -\omega_1 \\ -\omega_2 & \omega_1 & 0 \end{pmatrix}, \tag{20}$$

where the angular rotation rates ω_i of the e-frame w.r.t. the b-frame are obtained from Eq. (11) by subtracting the earth rotation rate, i.e.

$$(\omega_1, \omega_2, \omega_3)^{\mathrm{T}} = \omega^{\mathrm{b}} - C^{\mathrm{b}}_{\mathrm{e}} \cdot (0, 0, \omega_{\mathrm{E}})^{\mathrm{T}} =: \omega^{\mathrm{b}}_{\mathrm{be}}. \tag{21}$$

The differential equation of (19) shall be solved with Quaternions. Jekeli transformed the 3×3 matrix equation of (19) to the 4×1 vector equation

$$\dot{q} = \frac{1}{2} A_q q, \tag{22}$$

with the quaternion q and the matrix of angular velocities A_q. The latter one is given by

$$A_q = \begin{pmatrix} 0 & \omega_1 & \omega_2 & \omega_3 \\ -\omega_1 & 0 & \omega_3 & -\omega_2 \\ -\omega_2 & -\omega_3 & 0 & \omega_1 \\ -\omega_3 & \omega_2 & -\omega_1 & 0 \end{pmatrix}. \quad (24)$$

We performed the integration of the Quaternion with the third order Runge-Kutta method (see Jekeli [8]), i.e. the Quaternion at time t_{n+1} is given by

$$\begin{aligned} q(t_{n+1}) &= q(t_n + h) \quad (25) \\ &= q(t_n) + h \cdot \left(\frac{1}{6}\delta q_0 + \frac{2}{3}\delta q_1 + \frac{1}{6}\delta q_2 \right), \end{aligned}$$

where $h = 2\delta t$ denotes the integration time and δq_0, δq_1 and δq_2 denote the coefficients given by

$$\begin{aligned} \delta q_0 &= \frac{1}{2} A_q(t_n) q(t_n) \\ \delta q_1 &= \frac{1}{2} A_q(t_n + \frac{h}{2}) \left(q(t_n) + h/2 \delta q_0 \right) \\ \delta q_2 &= \frac{1}{2} A_q(t_n + h) \left(q(t_n) - h\delta q_0 + 2h\delta q_1 \right). \quad (26) \end{aligned}$$

Once the integrated quaternion is determined, we can transform it back to a rotation matrix and obtain Eq. (23) according to Jekeli [8].

Multiplying from the left by $(C_{\mathrm{n}}^{\mathrm{e}})^{-1}$ yields the transformation matrix from the b-frame to the n-frame, i.e.

$$C_{\mathrm{b}}^{\mathrm{n}}(t_{n+1}) = (C_{\mathrm{n}}^{\mathrm{e}}(t_{n+1}))^{-1} C_{\mathrm{b}}^{\mathrm{e}}(t_{n+1}). \quad (27)$$

The roll angle is then given by

$$\phi(t_{n+1}) = \arctan\left(\frac{(C_{\mathrm{b}}^{\mathrm{n}}(t_{n+1}))_{(2,3)}}{(C_{\mathrm{b}}^{\mathrm{n}}(t_{n+1}))_{(3,3)}} \right), \quad (28)$$

and the pitch angle follows as

$$\theta(t_{n+1}) = -\arcsin((C_{\mathrm{b}}^{\mathrm{n}}(t_{n+1}))_{(1,3)}). \quad (29)$$

The yaw angle/ heading is obtained as

$$\psi(t_{n+1}) = \arctan\left(\frac{(C_{\mathrm{b}}^{\mathrm{n}}(t_{n+1}))_{(1,2)}}{(C_{\mathrm{b}}^{\mathrm{n}}(t_{n+1}))_{(1,1)}} \right). \quad (30)$$

Constrained integer tree search

The cycle corrections ΔN_{12} and the baseline $\vec{b}_{12}$ are determined from the measurements of Eq. (8) by a constrained integer least-squares estimation, i.e.

$$\min_{\vec{b}_{12}, \Delta N_{12}} \|z - H\vec{b}_{12} - A\Delta N_{12}\|^2_{\Sigma_z^{-1}} \quad \text{s.t.} \quad \|\vec{b}_{12}\| = l. \quad (31)$$

The minimization over ΔN_{12} implies a search of all CSC candidates inside a predefined search space volume χ^2. We perform a Lagrange optimization and write the search as an inequality (see Teunissen [1]-[2]), i.e.

$$\begin{aligned} \min_{\vec{b}_{12}} \Big(&\|z - Hb_{12} - A\Delta N_{12}\|^2_{\Sigma_z^{-1}} \\ &+ \mu \cdot (\|b_{12}\|^2 - l^2) \Big) \leq \chi^2, \quad (32) \end{aligned}$$

with Lagrange parameter μ. The weighted sum of squared measurement residuals was decomposed by Teunissen into three terms: a weighted sum of squared ambiguity (here: cycle slip) residuals, a weighted sum of squared baseline residuals and a term for the irreducible noise, i.e.

$$\begin{aligned} &\|z - Hb_{12} - A\Delta N_{12}\|^2_{\Sigma_z^{-1}} \\ &\quad = \|\Delta\hat{N}_{12} - \Delta N_{12}\|^2_{\Sigma^{-1}_{\hat{N}_{12}}} + \|\check{b}_{12}(\Delta N_{12}) - b_{12}\|^2_{\Sigma^{-1}_{\check{b}_{12}}} \\ &\qquad + \|P_{\bar{A}}^{\perp} P_H^{\perp} z\|^2_{\Sigma_z^{-1}}, \quad (33) \end{aligned}$$

with $P_H^{\perp}$ being the orthogonal projector on the space of H and $\bar{A} = P_H^{\perp} A$. The first term on the right side of Eq. (33) can be further developed by using a triangular decomposition, which leads to a weighted sum of squared *conditional* ambiguity residuals, i.e.

$$\|\Delta\hat{N}_{12} - \Delta N_{12}\|^2_{\Sigma^{-1}_{\Delta\hat{N}_{12}}} = \sum_{l=1}^{k} \frac{(\Delta N_{12}^l - \Delta\hat{N}_{12}^{l|1,\ldots,l-1})^2}{(\sigma_{\Delta\hat{N}_{12}^{l|1,\ldots,l-1}})^2}, \quad (34)$$

where the conditional cycle slip corrections $\Delta\hat{N}_{12}^{l|1,\ldots,l-1}$ and the conditional standard deviations $\sigma_{\Delta\hat{N}_{12}^{l|1,\ldots,l-1}}$ were derived e.g. by Teunissen in [1]. Setting Eq. (34) into Eq. (33) and setting the obtained error decomposition into the inequality of (32) yields

$$\begin{aligned} \frac{(\Delta N_{12}^k - \Delta\hat{N}_{12}^{k|1,\ldots,k-1})^2}{\sigma^2_{\Delta\hat{N}_{12}^{k|1,\ldots,k-1}}} &\leq \chi^2 - \|P_{\bar{A}}^{\perp} P_H^{\perp} z\|^2_{\Sigma_z^{-1}} \\ &- \sum_{l=1}^{k-1} \frac{(\Delta N_{12}^l - \Delta\hat{N}_{12}^{l|1,\ldots,l-1})^2}{(\sigma_{\Delta\hat{N}_{12}^{l|1,\ldots,l-1}})^2} \\ &- \min_{\vec{b}_{12}, \mu} \left(\|\check{\vec{b}}_{12}(N_{12}) - \vec{b}_{12}\|^2_{\Sigma^{-1}_{\check{\vec{b}}_{12}}} + \mu \cdot (\|\vec{b}_{12}\|^2 - l^2) \right). \quad (35) \end{aligned}$$

There are two important aspects to note: First, the right side of inequality (35) only depends on the *previous* CSC, i.e. ΔN_{12}^l with $l < k$, which enables a sequential tree search as shown in Fig. 5.

Secondly, the Lagrange optimization forces the baseline estimate to fulfill the length constraint. This implies that the

$$C_{\mathrm{e}}^{\mathrm{b}}(t_{n+1}) = \begin{pmatrix} q_a^2 + q_b^2 - q_c^2 - q_d^2 & 2(q_b q_c - q_a q_d) & 2(q_b q_d + q_a q_c) \\ 2(q_b q_c + q_a q_d) & q_a^2 - q_b^2 + q_c^2 - q_d^2 & 2(q_c q_d - q_a q_b) \\ 2(q_b q_d - q_a q_c) & 2(q_c q_d + q_a q_b) & q_a^2 - q_b^2 - q_c^2 + q_d^2 \end{pmatrix} \quad (23)$$

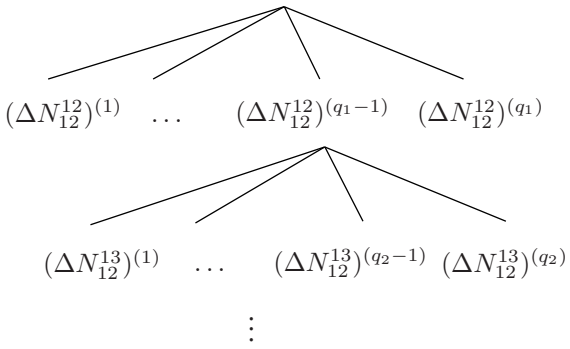

Fig. 5: Integer tree search for cycle slip correction

weighted sum of squared baseline residuals no longer vanishes. Thereby, the search space volume for the CSC candidates is substantially reduced compared to the unconstrained search.

Solving the inequality (35) yields a lower and an upper bound on the search interval for the k-th ambiguity, i.e.

$$\begin{aligned} \Delta N_{12}^{k} &\geq \Delta \hat{N}_{12}^{k|1,\ldots,k-1} - \sigma_{\Delta \hat{N}_{12}^{k|1,\ldots,k-1}} \sqrt{R} \\ \Delta N_{12}^{k} &\leq \Delta \hat{N}_{12}^{k|1,\ldots,k-1} + \sigma_{\Delta \hat{N}_{12}^{k|1,\ldots,k-1}} \sqrt{R}, \end{aligned} \quad (36)$$

with R being the right side of (35). Let us now perform the minimization in the last row of (35). We start by setting the derivative w.r.t. $\vec{b}_{12}$ to zero, which leads to the baseline estimate

$$\hat{b}_{12}(\mu) = (\Lambda(\mu))^{-1} \Sigma_{\check{b}_{12}}^{-1} \check{b}_{12}(N_{12}), \quad (37)$$

with $\Lambda(\mu) = \Sigma_{\check{b}_{12}}^{-1} + \mu 1$. Setting $\hat{b}_{12}(\mu)$ into the length constraint results in a root-finding problem:

$$f(\mu) = \|\hat{b}_{12}(\mu)\|^2 - l^2 \stackrel{!}{=} 0. \quad (38)$$

The roots are determined iteratively with the Newton method, i.e.

$$\mu^{(n+1)} = \mu^{(n)} - f(\mu) / \frac{\partial}{\partial \mu} f(\mu) \Big|_{\mu=\mu^{(n)}}, \quad (39)$$

which requires the derivative of a matrix inverse. We know that

$$\Lambda(\mu) \cdot (\Lambda^{-1}(\mu)) \stackrel{!}{=} 1. \quad (40)$$

Taking the derivative w.r.t. μ yields:

$$\frac{\partial}{\partial \mu} \Lambda(\mu) \cdot (\Lambda^{-1}(\mu))) + \Lambda(\mu) \cdot \frac{\partial}{\partial \mu} (\Lambda^{-1}(\mu))) \stackrel{!}{=} 0, \quad (41)$$

which is solved for $\partial / \partial \mu (\Lambda^{-1}(\mu))$:

$$\frac{\partial}{\partial \mu} (\Lambda^{-1}(\mu))) = -(\Lambda^{-1}(\mu)) \frac{\partial}{\partial \mu} \Lambda(\mu) \cdot (\Lambda^{-1}(\mu))), \quad (42)$$

and can be easily determined in closed form.

MEASUREMENT RESULTS

Two low-cost single frequency GPS patch antennas were mounted on the roof of a car along its longitudinal axis as shown in Fig. 1. The baseline length was 1.45 m. The antennas were connected to two u-blox LEA 6T GPS receivers, which provide both code and carrier phase measurements. We also used the chip MPU 9150 of Invensense, which includes both a three-axes accelerometer and a three-axes gyroscope and was accessed by an own circuit. Fig. 6 shows the complete vehicle track.

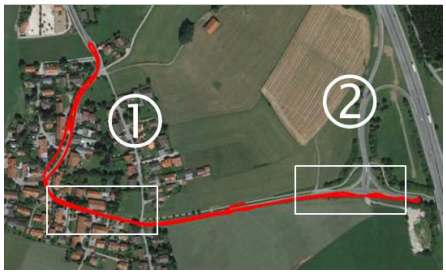

Fig. 6: Map of complete vehicle track: the section (1) is in a high multipath environment. Section (2) includes a slalom drive with high receiver dynamics.

The section labeled by (1) is enlarged in Fig. 7 and includes a narrow street passage where all satellite signals are two times shadowed by trees.

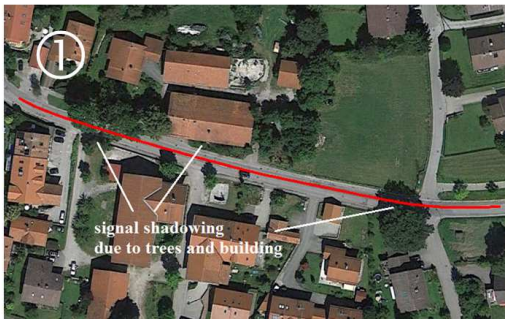

Fig. 7: Section (1) of vehicle track corresponds to the time interval $[36\,\mathrm{s},\ 56\,\mathrm{s}]$ of the total track of Fig. 6, and includes a narrow street passage surrounded by trees and buildings.

The section labeled by (2) is enlarged in Fig. 8 and includes a slalom drive with high receiver dynamics.

The signal shadowing by trees in Fig. 7 reduces the received signal power and causes numerous cycle slips. Fig. 9 shows the PRNs (without the reference satellite) that are affected by a cycle slip at a certain epoch. The cycle slips were detected with the proposed search algorithm using both GPS and INS measurements and the baseline length a priori information. One can observe that the 5 visible satellites are affected by numerous cycle slips and that several satellites are also affected simultaneously by cycle slips.

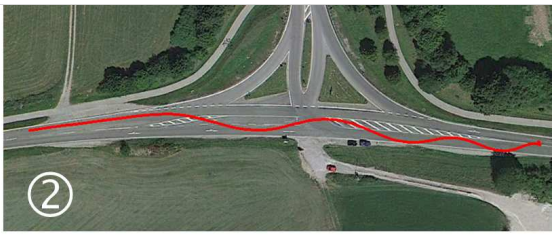

Fig. 8: Section (2) of vehicle track corresponds to the time interval $[240\ \mathrm{s},\ 255\ \mathrm{s}]$ of the total track of Fig. 6, and includes a slalom drive with high receiver dynamics.

Tab. 2 shows the relationship between the frequency of cycle slips and the satellite elevation for our 5 min test drive. The satellites of lower elevation showed more cycle slips than the ones of higher elevation but all satellites were affected by a significant number of cycle slips.

PRN	number of cycle slips	satellite elevation
21	37	44.5°
25	99	35.0°
27	19	60.6°
30	62	42.5°
31	54	50.5°

Tab. 2: Cycle slip statistics: The satellites of lower elevation show more cycle slips than the ones of higher elevation but all satellites are affected by frequent cycle slips.

Tab. 3 gives an insight into the simultaneous occurrence of cycle slips at multiple satellites. 31 out of 1500 epochs were affected by two simultaneous cycle slips and 2 epochs showed 3 satellites with simultaneous cycle slips. We also observed some epochs where all satellites were affected by cycle slips. Such events could be prevented by vector tracking loops as described in [13]. However, all satellites (or, in a few cases, all except one satellite) were showing the same cycle slip. This indicates that the cycle slips were most likely caused by a single cycle slip of the reference satellite (and, in a few cases, one additional cycle slip at another satellite).

number of epochs	number of simultaneous cycle slips
171	1
31	2
2	3
3	4
4	5

Tab. 3: Statistics of cycle slips: 171 epochs were affected by one cycle slip, which corresponds to one cycle slip every 2 s on average. There were even 4 epochs, where cycle slips were observed simultaneously at all satellites.

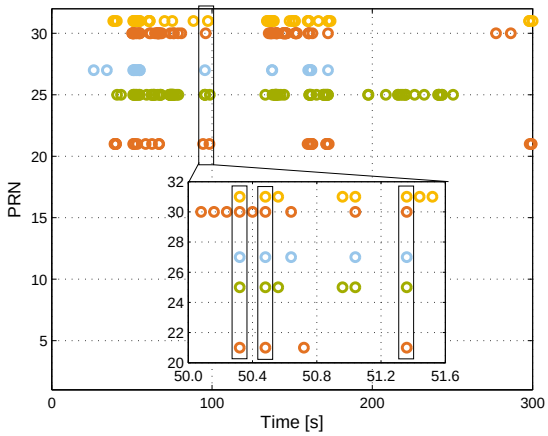

Fig. 9: Numerous cycle slips can be observed throughout the measurement test. In the narrow street passage of (1), trees are bridging the road and cause cycle slips at 5 satellites simultaneously.

Let us now analyze the benefit of the GPS/ INS-coupled cycle slip correction (CSC) over the pure GPS-based CSC for the complete receiver track of Fig. 6. Fig. 10 shows the fixed phase residuals after GPS only based CSC for all available double differences. Numerous cycle slips were corrected but there remain occasional jumps up to almost 1 m due to wrongly corrected or missed cycle slips.

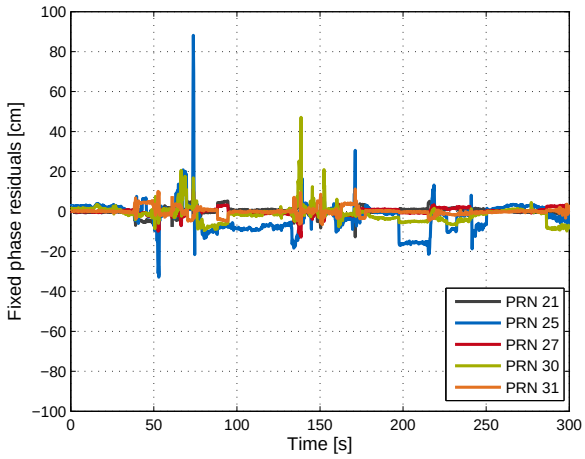

Fig. 10: Fixed phase residuals *after* GPS-based cycle slip detection and correction: Numerous cycle slips are corrected which results in lower residuals. However, there still remain undetected cycle slips.

Fig. 11 shows the fixed phase residuals after GPS/ INS-coupled CSC. One can observe that the residuals are reduced to less than $\lambda/2$ for all satellites throughout the measurement period. We conclude that the acceleration and angular rotation rate measurements and the baseline length a

priori information enable a reliable detection and correction of cycle slips.

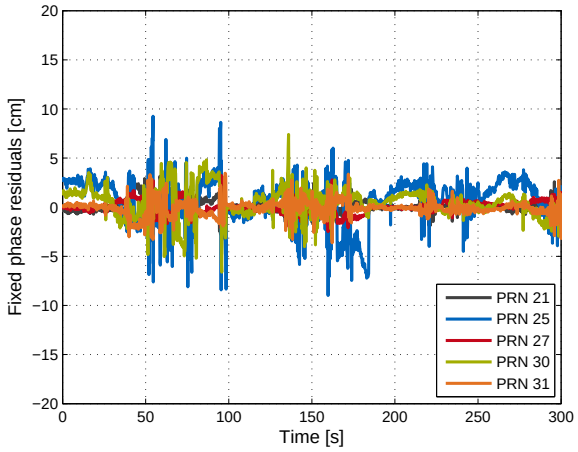

Fig. 11: Fixed phase residuals *after* GPS/ INS-based cycle slip detection and correction: The fixed phase residuals are reduced to less than $\lambda/2$ for all satellites throughout the measurement period.

Fig. 12 compares the heading estimates using GPS-only CSC with the heading estimates using joint GPS/ INS CSC. The two enlarged sections refer the vehicle tracks of Fig. 7 and Fig. 8. In the first section, we can observe some jumps in the GPS-only based heading at the beginning and end of the section. At these epochs, the car was driving below the two depicted trees in Fig. 7, and some cycle slips were missed or wrongly corrected leading to heading errors of up to 10 degrees. Similarly, the GPS-based CSC does not properly correct some cycle slips around 160 s resulting in heading errors of up to 20 degrees for 100 s. The INS/ GPS-coupled CSC enables an *instantaneous* and *reliable* correction of all cycle slips and, thereby, a precise heading estimation with an accuracy of $0.5°/$ baseline length [m].

ACKNOWLEDGMENT

The authors are deeply grateful that Philipp Berthold, Noaya Oku, Jane Jean Kiam and Juan Carlos Venegas made the circuit design, the board assembly, and the implementation of numerous algorithms for the Position and Attitude Determination (PAD) system of ANAVS.

CONCLUSION

Autonomous driving of cars requires a precise position and attitude information in real-time at low cost. The attitude can be derived from the double difference phase measurements of two low-cost GPS receivers. However, there is a need for reliable integer ambiguity resolution and cycle slip detection and correction.

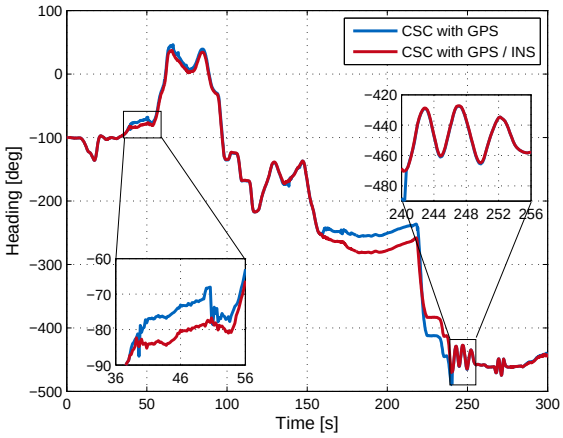

Fig. 12: Heading estimation with GPS-only CSC and joint GPS/ INS CSC: If only GPS measurements are used, some cycle slips are missed or wrongly corrected leading to heading errors of up to 20 degrees for time spans up to 100 s. The use of a low-cost IMU enables a reliable correction of all cycle slips and, thereby, a precise heading estimation.

In this paper, a cycle slip correction search algorithm was described, which jointly considers the double difference phase measurements from all visible satellites, the gyroscope and acceleration measurements, and the baseline length a priori information. The proposed method finds the optimum trade-off between minimizing the squared measurement residuals and minimizing the squared baseline length residuals. Various test drives have been conducted and measurement results showed that a reliable detection and correcting of cycle slips is feasible both in sections with substantial signal shadowing (e.g. below trees) and in sections with high receiver dynamics. The obtained heading accuracy was in the order of $0.5°/$ baseline length [m].

REFERENCES

[1] P. Teunissen, The least-squares ambiguity decorrelation adjustment: a method for fast GPS ambiguity estimation, *J. of Geodesy*, vol. 70, pp. 65-82, 1995.

[2] P. Teunissen, The LAMBDA method for the GNSS compass, *Art. Satellites*, vol. 41, nr. 3, pp. 89-103, 2006.

[3] P. Teunissen, Integer least-squares theory for the GNSS compass, *J. of Geodesy*, vol. 84, pp. 433-447, 2010.

[4] P. Henkel, G. Giorgi and C. Günther, Precise Attitude Determination with Low-Cost Satellite Navigation Receivers, *submitted to IEEE Trans. on Vehicular Technology*, 2013.

[5] P. Henkel and N. Oku, Heading determination with Integer Ambiguity Resolution for Low-Cost GPS/

INS, *Internat. Association of Geodesy Symposia*, Proc. of VIII Hotine-Marussi Symposium, Rome, Italy, Jun. 2013.

[6] P. Henkel and J. Kiam, Maximum A Posteriori Probability Estimation of Integer Ambiguities and Baseline, *IEEE Proc. of 55-th ELMAR Symposium*, Zadar, Croatia, Sep. 2013.

[7] P. Henkel, J. M. Cardenas and P. Jurkowski, Cascaded Heading Estimation with Phase Coasting. *IEEE Proc. of 54-th ELMAR Symposium*, pp. 283–286, Zadar, Croatia, Sep. 2012.

[8] C. Jekeli, Inertial Navigation Systems With Geodetic Applications, *Verlag de Gruyter*, 2001.

[9] P. Jurkowski, P. Henkel, G. Gao, and C. Günther, Integer Ambiguity Resolution with Tight and Soft Baseline Constraints for Freight Stabilization at Helicopters and Cranes, *Proc. of ION Intern. Techn. Meet.* (ION ITM), San Diego, USA, pp. 336-346, Jan. 2011.

[10] P. Henkel, P. Jurkowski and C. Günther, Differential integer ambiguity resolution with Gaussian a priori knowledge and Kalman filtering, *Proc. of 24th ION Intern. Techn. Meet.* (ION-GNSS), Portland, USA, pp. 3881-3888, Sep. 2011.

[11] P. Henkel and C. Günther, Reliable Integer Ambiguity Resolution with Multi-frequency Mixed Code Carrier Combinations, *Journal of Global Positioning Systems*, Vol.9, No. 2, pp. 90-103, 2010.

[12] P. Henkel and C. Günther, Partial integer decorrelation for optimum trade-off between variance reduction and bias amplification. *J. of Geodesy*, vol. 84, iss. 1, pp. 51-63, 2010.

[13] P. Henkel, K. Giger and C. Günther, Multi-satellite, multi-frequency Vector Phase Locked Loop for Robust Carrier Tracking, *IEEE J. of Selected Topics in Signal Processing* (J-STSP), Special Issue on Advanced Signal Processing for GNSS and Robust Navigation, vol. 3, nr. 4, pp. 674-681, 2009.